PHYSICS

Theory cracks old data: Rovibrational energy levels of *ortho*H_2–CO derived from experiment

Marcin Stachowiak[1], Ewelina Grabowska[1], Xiao-Gang Wang[2], Tucker Carrington Jr.[2], Krzysztof Szalewicz[3], Piotr Jankowski[1]*

Measurements of rovibrational spectra of clusters provide physical insight only if spectral lines can be assigned to pairs of quantum states, and further insight is obtained if one can deduce the quantitative energy-level pattern. Both steps can be so difficult that some measured spectra remain unassigned, one example is *ortho*H_2–CO. To extend the scope of spectroscopic insights, we propose to use theoretical information in interpretation of spectra. We first performed high accuracy, full-dimensional calculations of the *ortho*H_2–CO spectrum, at the highest practically achievable levels of electronic structure theory and quantum nuclear dynamics. Then, an iterative, theory-guided method developed here allowed us to fully interpret the spectrum of *ortho*H_2–CO, extending the range of van der Waals clusters for which spectroscopy can provide physical insights.

INTRODUCTION

Spectroscopy is among the most important methods of probing matter, it is also one of the most precise methods. For van der Waals (vdW) clusters, even the smallest ones, this precision cannot be yet matched by theory. For example, for the H_2–CO complex discussed here, the energies of most infrared (IR) transitions (line positions) are measured with precision of 0.0005 cm^{-1} (*1*), while the *para*H_2–CO transitions computed in (*2*), among the most accurate for any vdW dimer, have a root mean square error (RMSE) of 0.0081 cm^{-1} with respect to the experimental transitions shifted by the (experimental) value of CO fundamental (*3*). However, in some cases, spectroscopy measurements are hard to assign and therefore to interpret. Without proper interpretations, these measurements are of very limited value. In particular, a measurement of IR spectra of a vdW cluster often results in a "forest of spectral lines", as in the case of the *ortho*H_2–CO experimental spectrum shown in Fig. 1 (top row). Clearly, it is very difficult to identify the two energy levels from which a given spectral line originates.

Interpretation of the spectrum of H_2–CO is of great interest due to the importance of this dimer. It is obviously prominent in astrophysics because H_2 and CO are, respectively, the most abundant and the second most abundant molecules in space. Because H_2 is difficult to observe directly, easy to detect CO serves as an H_2 tracer (*4*). This requires an assumption that the CO-to-H_2 density ratio is approximately constant in space. This ratio is usually assumed to be equal to 10^{-4}, an assumption that is hotly debated (*4*–*7*). Information on this ratio and its variation in space can be inferred from observations of the H_2–CO complex, but these attempts (*8*, *9*) have been unsuccessful so far. The search for this dimer may become successful with updated, more precise devices including the James Webb Space Telescope (*10*). The detection of H_2–CO in the cold interstellar medium would also serve as a sensitive indicator of temperature. Because astronomical observations record a mixture of *para*H_2–CO and *ortho*H_2–CO spectra, full interpretation of both is needed to guide the observations, particularly because the latter spectrum is much denser. Furthermore, inelastic collisions of CO with H_2 play a key role in establishing the observed molecular populations in regions that are not in local thermodynamic equilibrium and theoretical calculations of the relevant cross sections use the same potential energy surfaces (PESs) as the investigations of the bound states of H_2–CO (*11*). This complex is also of interest in several fields of science beyond astrophysics. For instance, it was studied, both theoretically and experimentally, in the context of the detection of superfluidity in the *para*H_2 clusters (*12*). Moreover, H_2–CO is an important model system for vdW interactions, as it is a molecular dimer with interactions partly similar to those of rare gases: The negative dispersion energy dominates for most intermonomer separations R, while for small R, the positive exchange-repulsion energy becomes larger in magnitude. However, in contrast to rare gases, the electrostatic interactions, although smaller in magnitude than the dispersion and exchange ones (*13*), affect the depth and the position of the vdW minimum. This is a similar physical origin of binding to that between aromatic hydrocarbons. Thus, a better characterization of H_2–CO should help in understanding these complex systems, for which our intuitions remain undeveloped.

Interpretation of observed spectra can be accomplished at two levels. At the first level, one can identify qualitatively (in terms of quantum numbers) the energy levels associated with a given spectral line. This identification is performed on the basis of characteristic spectral patterns, and usually only a subset of lines can be assigned. At the next level, one can determine quantitatively the relative energies of all levels from which the spectral transitions stem. The latter is an ultimate interpretation of spectra and brings an abundance of physical insight into investigated systems. In particular, one can fit an empirical PES to these data, getting information about the nature of intermolecular interactions. The different possible levels of spectral interpretations are well illustrated on the example of H_2–CO. Observations of this complex date back to 1967 (*14*–*16*), and the 1998 IR experiment by McKellar (*1*) achieved the ultimate interpretation of *para*H_2–CO, i.e., the quantitative pattern of the rovibrational energy levels was deduced from experiment, and still provides the benchmark values. These energy levels were much more accurate than those from theoretical investigations of that time (*13*, *17*, *18*): The best theory versus experiment RMSE on the bound energy levels was 0.4 cm^{-1} (*13*). As the quality of ab initio PESs gradually improved, this RMSE dropped

[1]Faculty of Chemistry, Nicolaus Copernicus University in Toruń, Gagarina 7, 87-100 Toruń, Poland. [2]Chemistry Department, Queen's University, Kingston, Ontario K7L 3N6, Canada. [3]Department of Physics and Astronomy, University of Delaware, Newark, DE 19716, USA.
*Corresponding author. Email: piotr.jankowski@umk.pl

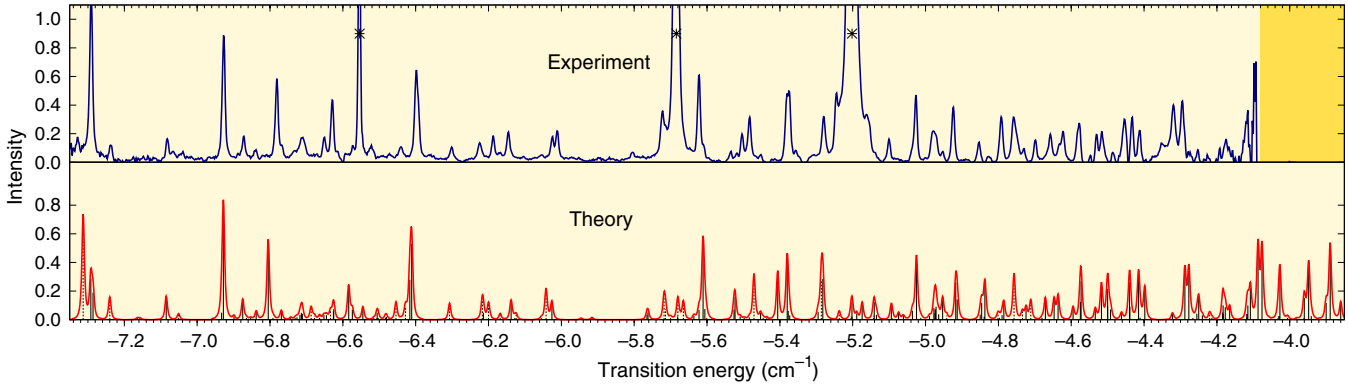

Fig. 1. A partial comparison of experimental and theoretical IR spectra of *ortho*H_2–CO. Continuous lines: Measured spectrum (blue, top row) (*2*) and the theoretical one (red, bottom row) from the present work; solid (dashed) vertical bars under the peaks: transitions between two bound (involving at least one resonance) rovibrational states; asterisks: various isotopologues CO monomer lines; yellow-shaded area: region where measurements of the H_2–CO spectra were not possible; zero of energy: 2143.2711 cm^{-1}, the $v = 0 \rightarrow 1$ vibrational frequency of the isolated CO monomer.

to 0.05 cm^{-1} in 2005 (*19*) and to 0.005 cm^{-1} in 2012 (*2*, *20*) (in both cases now including also the resonance states), small errors compared to the dissociation energy of about 20 cm^{-1}. The latter error constitutes one of the best agreements of theory with experiment for spectra of vdW molecules. Spectral measurements were also performed in the millimeter-wavelength range of energies (*21*, *22*), directly relevant for astrophysical observations. In contrast to *para*H_2–CO, the *ortho*H_2–CO spectrum, also recorded in 1998 (*1*), remained completely unassigned for a long time. The reason was that the *ortho* spectrum is much more complicated than the *para* one due to different nuclear spin couplings in the two cases, resulting in the angular momentum quantum number of H_2, j_1, to be odd and even for *ortho*H_2 and *para*H_2, respectively. At sufficiently low temperature, j_1 is equal to 1 (a triply degenerate p-type state) for *ortho*H_2 and 0 (a spherically symmetric state) for *para*H_2. As the result, *ortho*H_2 motions can be coupled with CO motions in more ways than in the case of *para*H_2. The increased couplings also result in probing the PES more extensively. With the increased accuracy of the 2012 PES (*2*, *20*), denoted as V_{12}, an attempt was made to assign *ortho*H_2–CO spectrum. This attempt was partly successful as more than 200 IR transitions were assigned (of about 1000 possible reasonably strong transitions determined from theory), as well as 26 millimeter-wavelength transitions. These assignments were made by identifying transition-energy regions where the observed and theoretical spectra were so close to each other that the known theoretical characteristics of a line could be used to label an experimental line (see Fig. 1). However, despite notable efforts and the guidance from theory, only a small number of energy levels were deduced in subsets that could not be linked together.

We present here work aimed at cracking the problem of deducing energy levels from the *ortho*H_2–CO spectra. There are two areas where progress has been made: increased accuracy of theoretical spectra including line intensities and the development of a better deduction protocol. An obvious improvement of theory is the extension of spectral calculations from four dimensions (4D) (*2*, *20*) to full dimensionality (6D), and we present here such an extension. The previous level-deduction protocol was essentially a single-sweep trial and error procedure from lines to levels. The original level-deduction protocol developed here is iterative: The previously deduced energy levels are used to assign more lines, and then these newly assigned lines are used to deduce more levels. The effect of this effort has been an essentially complete interpretation of the *ortho*H_2–CO spectra: We were able to deduce from experiment the energies of 84% of all possible rovibrational levels. This is close to the maximum possible number since several spectral regions are not accessible to experiment.

RESULTS

Potential energy surface

The first step in our investigations was the development of a 6D PES. The most accurate published H_2–CO spectra were obtained from a 4D V_{12} surface (*2*, *20*). The ab initio calculations in (*2*, *20*) were actually performed on a 6D grid, although the intramonomer separations were probed only in a narrow range enabling numerical calculations of derivatives needed in the Taylor expansion method (*23*). The 6D surface was then averaged over the motions within monomers. The resulting 4D set of averaged interaction energies was fitted by an analytic function. In the present work, we have obtained an analytic 6D PES. 6D PESs for H_2–CO have been published previously (*24*–*26*) but used only in scattering and virial coefficients calculations. Because of the steep increase in the number of 6D grid points, necessitating the use of lower levels of theory, and due to higher fit uncertainties in 6D, 4D averages of these surfaces would be less accurate than V_{12}. Our 6D surface developed here, denoted as V_{23}, overcomes these problems. The interaction energies were computed in the same way as in (*27*). The uncertainty of these energies was estimated to be equal to 0.6 cm^{-1} relative to the exact relativistic adiabatic value or 0.8% of the total interaction energy at the global minimum (*20*). The interaction energies computed on a grid of 34,559 short-range and 11,265 long-range points were fitted by analytic functions (see the Supplementary Materials for details). The RMSE of the fit is 0.34 cm^{-1} on all points and 0.02 cm^{-1} for points with negative values of E_{int}, most important for spectra. The latter value can be compared to that of the 6D PES from (*26*) equal to 0.16 cm^{-1}. Clearly, a very substantial improvement has been achieved. The intermolecular interaction surface V_{23} supplemented by monomer potentials gives the total 6D PES denoted as U_{23}. A computer code calculating V_{23} is provided in the Supplementary Materials.

Nuclear motion calculations

The H_2–CO complex has six rovibrational degrees of freedom, and we have performed most of the calculations in full (6D) dimensionality. For some calculations, specified below, we used a reduced dimensionality PES, depending only on the four intermolecular degrees of freedom (4D). The simplest way to obtain a 4D PES is to fix the H—H and C—O bond lengths. A much better way (*28*) is to first obtain a 6D surface and then average it over the intramolecular bond lengths in a rovibrational state of each monomer, which is what we did. The 6D calculations of rovibrational spectra for the *para* and *ortho*H_2–CO systems have not been done before and are challenging because computing energies up to CO vibrational state with $v_2 = 1$ (at about 2000 cm^{-1}) requires using a very large rovibrational basis set. Numerically exact calculations for vdW dimers have been performed up to 12 dimensions (*29*), but the energy range involved was an order of magnitude smaller. Our calculations for the bound rovibrational states uses a discrete variable representation (DVR) basis for the radial coordinates and spherical harmonic type basis for the bends. The variational eigenproblem in the product of the two bases was solved using a symmetry-adapted Lanczos algorithm. The method is denoted as DSL (DVR + spherical + Lanczos) (*30*, *31*). The 6D rovibrational calculations were numerically converged to 0.0001 cm^{-1} for the lowest bound state with $v_2 = 0$ or $v_2 = 1$ and to much better than 0.001 cm^{-1} for all other bound states of *ortho*H_2–CO. The rovibrational states of H_2–CO are labeled by (J, P, $n_{J,P}$, v_2), where J is the rotational quantum number of the complex, P is its spectroscopic parity, and $n_{J,P}$ denotes consecutive states with these values of J and P. Further details of 6D rovibrational calculations are given in Methods.

For the resonance states, the 6D calculations are difficult and we instead did 4D scattering calculations. They are numerically converged to better than 0.001 cm^{-1} for all considered states. We have also performed 4D calculations for bound states to compare them to 6D ones. All 4D calculations used a 4D set of interaction energies computed on-the-fly from V_{23} (i.e., no analytic 4D fits were done). The same Taylor expansion method (*23*) as in (*2*, *20*) was applied in averaging over motions within the monomers, except that the values and derivatives of energy were computed from V_{23}. The resulting surfaces are denoted by $\langle V_{23}\rangle_{v1=0,v2=0,1}$ or in short as $\langle V_{23}\rangle$. We have used the BOUND and MOLSCAT programs (*32*) to perform the 4D rovibrational and scattering calculations (see the Supplementary Materials for details). All intensities were computed from 4D wave functions. For the quasibound states, the wave functions were obtained from the stabilization method (*2*, *20*). Because accuracy requirements for intensities are not as high as for line positions, this approach is fully satisfactory (also, the 6D and 4D approaches are nearly equally accurate, as discussed below).

Assessment of theoretical spectra

Stringent validations and error estimates of the computed spectra come from comparisons with experiment. A qualitative comparison of experimental *ortho*H_2–CO spectra data with the spectra from the 6D + 4D approach (V_{23} for bound states and $\langle V_{23}\rangle$ for resonances) is shown in Fig. 1 and in fig. S1. To easily see the differences between the two spectra, the range of the horizontal scale of fig. S1 is 1 cm^{-1} per panel. On the condensed plot of Fig. 1, the two spectra appear to be nearly identical, but fig. S1 shows that while many of strong lines closely overlap also at this scale, some lines are shifted up to about 0.06 cm^{-1}. This demonstrates the difficulties in assigning the experimental transitions.

To evaluate accuracy of the 6D + 4D calculations in quantitative terms, we first compare them to the experimental energy levels for *para*H_2–CO: The RMSE is 0.0051 cm^{-1} for all experimental levels with $v_2 = 0$ given in (*1*). Thus, this RMSE is virtually the same as 0.0054 cm^{-1} found in the 4D calculations of (*2*, *20*) with V_{12}. For the $v_2 = 1$ levels, the corresponding RMSEs are 0.0089 and 0.0069 cm^{-1}. Thus, both theoretical approaches are of similar accuracy with respect to experiment. In the case of *ortho*H_2–CO, we can compare the performance of the two methods on the list of 209 transitions initialy assigned in (*2*, *20*) and revised in the present work. The calculated RMSE between theoretical and experimental transitions is 0.0177 cm^{-1} for the 6D + 4D approach, virtually the same as the corresponding value of 0.0172 cm^{-1} obtained here from V_{12} in (*20*). In all cases discussed here, $\langle V_{23}\rangle$ spectra have similar RMSEs.

These virtually identical predictions from the V_{12}-based 4D, $\langle V_{23}\rangle$-based 4D, and V_{23}-based 6D + 4D calculations are quite astonishing. For the purposes of the present work, this shows that the quality of V_{23} in the rigid-monomer sector is the same as that of V_{12}. More generally, this shows that the monomer-flexibility effects beyond those included in $\langle V_{23}\rangle$ are negligible for H_2–CO at the present level of theory. Whereas similar conclusions were found in scattering calculations for this system (*25*), the present findings are at much higher level of precision. While calculations of all-dimensional PESs became quite popular in recent years, little is known about the importance of monomer-flexibility effects. To our knowledge, rigorous comparisons involving $\langle V\rangle$-type PESs have been performed earlier only for Ar-HF (*28*), i.e., between 2D and 3D approaches. Note that only the reduced-dimensionality PESs obtained from full-dimensionality ones by averaging over intramonomer motions provide such good agreement, the same is not true for rigid-monomer PESs computed at fixed intramonomer geometries. Although energy levels calculated on an averaged PES obtained with the Taylor expansion method may differ from those on a full-dimensional PES, more substantially for more strongly bound vdW dimers, it is encouraging that they are extremely close for H_2–CO. One can expect this closeness to be the case for other weakly bound vdW dimers as well. Rovibrational calculations on an averaged PES are much easier because, for dimers, there are at most six intermolecular coordinates. Whereas flexible monomer spectral calculations are only possible up to 12 dimensions, calculations with only the intermolecular coordinates are becoming routine.

An all-dimensional approach naturally predicts values of monomer properties within a dimer, such as shifts of intramonomer fundamental transitions due to intermolecular interactions. Our 6D approach gives −0.172 cm^{-1} (red) shift for the CO fundamental, which agrees very well with the experimental value of −0.179 cm^{-1} (*1*). This shift can be also computed in the 4D approach with $\langle V\rangle$-type PESs by comparing the dissociations energies from $v_2 = 0$ and $v_2 = 1$ surfaces. The calculation with $\langle V_{23}\rangle$ gives the value of −0.173 cm^{-1}, while the value computed in (*20*) was −0.176 cm^{-1}.

Deduction of experimental energy levels

The most essential improvement over the published work, which allowed us to find the experimental rovibrational energy levels of *ortho*H_2–CO, was the development of an iterative protocol for deducing energy levels from spectra. Our protocol consists of two similar but not identical stages. Each stage is composed of three steps: (1) assignment of experimental transitions, (2) deduction of experimental energy levels from the assigned transitions, and (3) generation of the spectrum from all the experimental levels deduced so far

(with theoretical intensities). Essential elements of our protocol are utilization of symmetries of the rovibrational wave functions and of the selection rules.

We started from the set of transitions assigned in (*20*). Our initial application of the protocol was not particularly successful. We realized that the reason could be that a few previous assignments are incorrect, and any misassigned lines wreak havoc in the level-deduction protocol. We have, therefore, critically reviewed the previous assignments (*20*) using the new theoretical values of line positions and intensities. We have also analyzed the experimental spectrum by fitting lines that theory indicated as resulting from overlapping transitions with a sum of Voigt profiles, assigning two or three transitions to a peak earlier assigned to a single transition energy. As the result of this reanalysis, we have rejected a few assignments, reducing their number to 209, and have corrected another few of them. The reduced list of 209 assigned transitions is given in table S1 and has been used as the input to step 2 of stage I. With the improved methodology, we could have assigned a number of new lines, but we wanted to start from the level used in (*20*) to compare the protocols.

The level-deduction procedure (step 2) used by us is similar to the standard combination differences method (*33*) and is illustrated in Fig. 2. In this method, one selects all transitions ending in a given energy level (J', P', $n'J'$,P', 1) and originating from a set of initial energy levels (J, P, $n_{J,P}$, 0), (J', P', $n'J'$,P', 1) ← (J, P, $n_{J,P}$, 0), and from the transition energies (in oval fields) calculates the relative energies of the levels with $v_2 = 0$. A group of transitions starting from a cluster of 4 rovibrational states with $v_2 = 0$ in the green panel and ending up in the (2,e,2,1) state gives us information about the energies of the three states relative to the (1,e,1,0) one. One can next find other clusters, such as that shown in the blue box, and link them together via common states, such as (3,e,3,0), into the cluster shown in the red box. We were able to construct a single large cluster of relative energy levels for each of the (J, P) symmetry blocks allowed by the selection rules, predicting 63% of all theoretically possible states.

In the third step of each stage, the experimental levels found in step 2 are used to generate all allowed transitions between these levels. The agreement with the previously assigned transitions provides a verification of the correctness of the deduction procedure. Moreover, the generated set of transitions allows one to assign a number of new transitions: 69 such transitions have been assigned in stage I. Note that these 69 transitions contain no information about energy levels that were not yet deduced. The closeness of the matching of these 69 generated transitions with the actual experimental transitions confirms indirectly the correctness of the already determined experimental energy levels involved in these transitions. This process is assisted by comparisons with the corresponding theoretical positions and intensities. It also identifies energy levels ending up mostly in transitions belonging to unobservable spectral regions (yellow regions of Fig. 1 and fig. S1 and therefore impossible to deduce from the experimental spectrum. For instance, the (4,f,5,0) state is active in six transitions with relative intensities larger than 0.01, one of them even as large as 0.47. However, five of these transitions are in the unobservable areas. The last one is overlapped by the strong $^{12}C^{17}O$ line at 8.6263 cm^{-1}. Thus, the experimental energy of the (4,f,5,0) state cannot be determined from the analyzed IR spectrum.

Conceptually, stage II was identical to stage I. The main difference is that we looked at one energy level at a time, used theoretical guidance more extensively, and iterated steps 1 to 3 several times. In the first step of each iteration, we picked one theoretical energy level whose experimental counterpart was missing and looked for

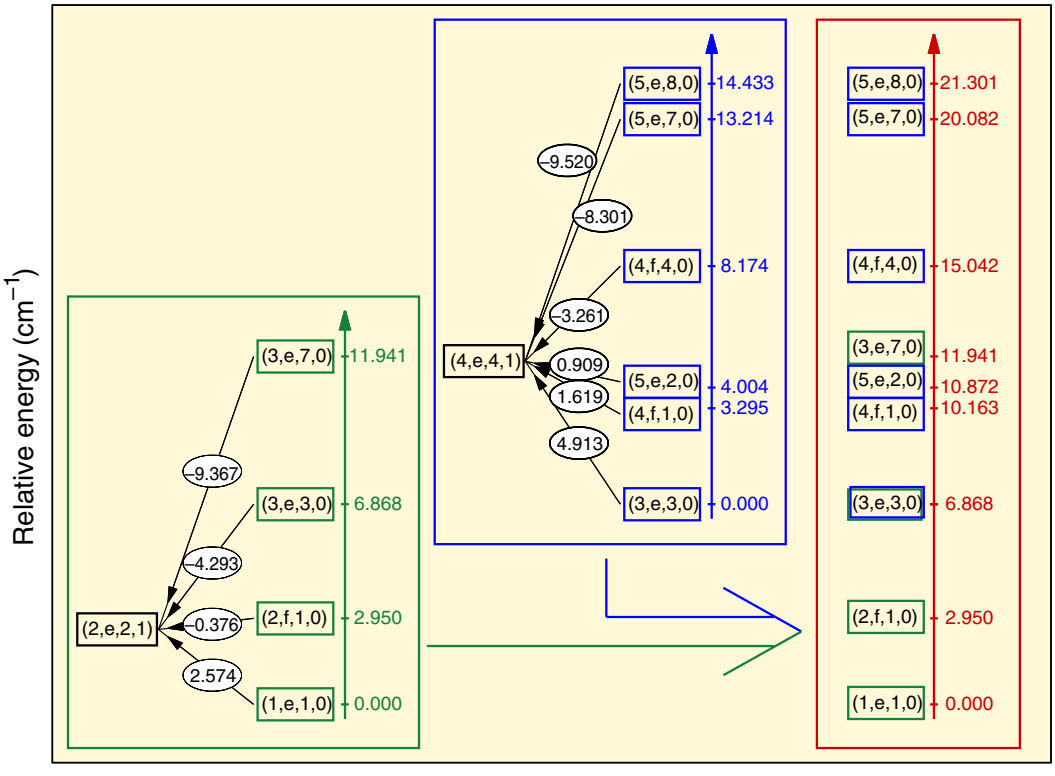

Fig. 2. Illustration of the protocol for deducing rovibrational energy levels from assigned IR transitions energies.

theoretical transition energies involving this state and all the levels that had an experimental counterpart. We compared each transition energy with the experimental spectrum near this transition. This focused survey of experimental spectrum allowed us to assign transitions that were too week or situated in a too dense region to allow an assignment in stage I. The stage II assignments are helped by the 69 lines assigned in stage I. This is possible in cases of a group of a few close-lying experimental lines corresponding to a similar group of theoretical lines. If some members of such a group are assigned, then the remaining experimental and theoretical lines can often be found to be related to each other. Even one newly assigned transition gives us immediately the experimental level corresponding to the chosen theoretical one, which constitutes step 2. In some cases, additional new experimental energy levels were obtained because it became possible to link previously unlinked clusters of transitions. In step 3, we used the extended set of experimental energy levels to generate experimental spectrum and compared this spectrum with the measured one (this comparison also sometimes led to assignment of new transitions). In this way, we could immediately validate our assignments in step 1 and possibly discard or correct them. In the next iteration, another theoretical level with missing experimental counterpart was picked. Overall, we were able to increase the number of experimental energy levels to 84% of all possible ones. For the $v_2 = 0$ case, we have found 56 experimental levels of odd parity of 66 levels predicted by theory (56 of 65 for even parity), whereas for the $v_2 = 1$ case, the corresponding numbers are 54/55 of 66/65. In Fig. 3, the diagram of the energy levels for $v_2 = 0$ is presented, and the numerical values for $v_2 = 0$ and 1 are given in tables S2 and S3, respectively. In all iterations of stage II, we assigned 41 transitions in step 1 and 35 ones in step 3. The latter transitions are marked by short red vertical arrows in the bottom rows of each panel of fig. S1. The total number of assigned lines is now 354 (209 + 69 + 41 + 35), much more than the total number of 219 experimental lines (assigned with a few mistakes) published in (*20*). All these transition energies are given in tables S4 and S5, whereas a complete list of calculated theoretical transitions is presented in table S6.

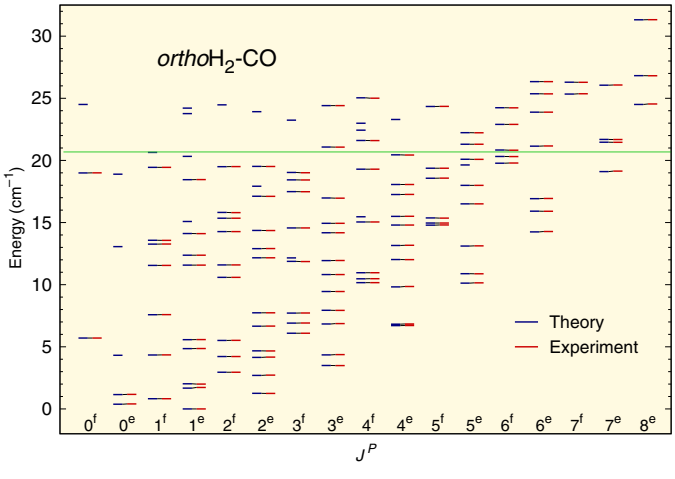

Fig. 3. Experimental and theoretical energy levels of *ortho*H_2–CO for $v_2 = 0$. The theoretical levels (in blue) are given relative to the lowest rovibrational state (1,e,1,0). The experimental levels (in red) are given relative to the corresponding experimental one. The green line marks the dissociation threshold.

Our deduction of 84% of the levels is close the limit for the existing experimental data. One can show from the comparison of theoretical and experimental spectra that the remaining 16% cannot be obtained because experimental transitions providing required information are very weak, or are obscured by much more intense lines, or lie in the ranges of energies not covered in the present experiment. Our work provides information to help plan a future experiment for *ortho*H_2–CO to fill the current gaps in the experimental energy pattern. One method could be to repeat the experiment at reduced pressure in the chamber, which makes the monomer lines narrower and reveals more features of the spectrum, as it was done (*20*) for *para*H_2–CO (although this change degrades the signal-to-noise ratio and can cause the transitions of low intensities to be lost in the background noise). The modern experimental techniques such as ultrahigh finesse cavity–enhanced laser spectroscopy (*34*) and spectroscopy in cryogenic regime (*35*) should achieve this narrowing without degrading the signal-to-noise ratio.

DISCUSSION

We have developed a synergistic method, which combines highest possible accuracy quantum mechanical calculations with analysis of experimental spectra to fully interpret the spectrum of the *ortho*H_2–CO complex. The computed spectrum was used to guide the process, which succeeded in deduction of experimental energy levels of this systems, the task that eluded all efforts in the past 25 years. A total of 84% of all possible levels have been found, while most of the remaining 16% cannot be deduced due to missing regions in the experimental spectrum (but they can be taken from theory). Our work provides, therefore, solid reference data for searches of H_2–CO in space, particularly because the generated transitions energies partly fill the gaps (maintaining experimental accuracy). Also, theoretical transition energies can be used in parts of the spectrum currently unobservable in the laboratory despite the fact that the theoretical data are less accurate. The methodology developed here extends applicability of spectroscopy to vdW clusters. Future applications to these clusters will increase understanding of these important systems and of the intermolecular interactions in general. Our calculations pushed the current limits of theory; in particular, we used a full-dimensional approach and the highest currently practical level of theory. The ab initio interaction energies on the 6D grid were computed for the first time at this high level of theory for grid points beyond the 4D cut of the PES. The analytic 6D fit is of high fidelity; in particular, in its regions probed in the calculations of spectra, the RMSE of the fit is several times smaller than the estimated uncertainty of the ab initio calculations. This high fidelity was possible due to our extensions of the previously used PES fitting methodology. The final theoretical spectrum was built from energy levels obtained in 6D quantum nuclear motion calculations for all bound states and from 4D calculations (with a 4D PES obtained by averaging the 6D PES) for all resonance states.

METHODS

Calculations of interaction energies

The interaction energies were computed in the same way as in (*27*), i.e., using the supermolecular approach, $E_{int} = E_{H2-CO} - E_{H2} - E_{CO}$, where E_X is the total electronic energy of system X, levels of theory up to the coupled clusters method with single, double, triple, and

noniterated quadruple excitations [CCSDT(Q)], basis sets up to the augmented quintuple-zeta quality, and extrapolations to the complete basis set limits. Because $r_1 = r_{H-H}$ and $r_2 = r_{C-O}$ are the same in calculations of E_{H2} and E_{CO}, respectively, as in E_{H2-CO}, the limit of E_{int} for the intermolecular separation $R \to \infty$ is zero for any value of the other coordinates. All electrons were correlated, and the counterpoise correction for the basis set superposition error was used.

6D fit of PES

The interaction energies were computed on a grid of 34,559 points. In addition, 11,265 interaction energies were computed for R larger than 13.5 bohr using a lower level of theory, adequate in this region: Only the CCSD(T) method and basis sets up to the augmented quadruple-zeta size were used. The interaction energies were fitted by an analytic function that consisted of short- and long-range parts, with a smooth switching at R values between 10 and 12 bohrs, using the switching function from (*36*). The form of the long-range part was taken from (*25*), but the parameters were refitted to the present set of interaction energies at large R. The short-range part was taken in the form of a sum of products of exponentials $e^{-\alpha r_{ab}}$, where r_{ab} are atom-atom distances (*37*, *38*). In contrast to most published work that uses the same α for all terms, we used four different, optimized values. The number of linear parameters was 1198. The intermolecular interaction surface V_{23} was supplemented by monomer potentials V_{H2} and V_{CO} (*39*–*41*).

On-the-fly calculation of interaction energies in 4D

The calculations of interaction energies in 4D were performed on-the-fly, i.e., for each point in 4D coordinates needed by a nuclear dynamics program. The averaging of the V_{23} surface was over the ground vibrational state of H_2, $v_1 = 0$, and two lowest-lying vibrational states of CO, $v_2 = 0, 1$. In contrast to earlier work, the state $v_1 = 0, j_1 = 1$ was used for *ortho*H_2–CO, which improved agreement with experiment.

Full-dimensional rovibrational calculations

The 6D rovibrational Schrödinger equation was solved with a product basis and the symmetry-adapted Lanczos method (*42*, *43*). The method is explained in (*30*, *31*, *44*, *45*). The product basis functions are

$$f_{\alpha_0}(r_0) f_{\alpha_1}(r_1) f_{\alpha_2}(r_2) u^{JM\bar{p}}_{j_1 j_2 m_2 K}(\theta_1, \theta_2, \phi; \alpha, \beta, \gamma) \quad (1)$$

where $f_{\alpha i}(r_i)$ is a DVR function, $u^{JM\bar{p}}_{j_1 j_2 m_2 K}$ is a parity-adapted bend-rotation function; α, β, γ are Euler angles specifying the orientation of the body-fixed frame in the space-fixed frame; r_0 is the intermonomer distance; r_1 and r_2 are the monomer bond lengths; θ_1, θ_2, ϕ are polyspherical angles; M is the projection of J; m_i is the projection of j_i; and $K = m_1 + m_2$. The $\bar{p}$ index denotes the parity case, with $\bar{p} = 0$ and $\bar{p} = 1$ corresponding to even ($p = 1$) and odd ($p = -1$) parity, respectively. In turn, p is related to the spectroscopic parity P used to label the rovibrational states by $p = (-1)^J P$.

Basis set parameters are chosen to ensure energy levels are converged. Potential optimized DVR (PODVR) bases (*46*, *47*) are used for r_1 and r_2 coordinates. With the basis II specified in table S7, all the bound states (for the *para* and *ortho* cases) are converged to within 0.0001 cm^{-1} compared to the much larger benchmark basis I also characterized in table S7, except for a few bound states near the dissociation limit and the resonance states. Thus, basis II is very efficient, being 37 times smaller than the benchmark one.

The IR spectrum was recorded in the vicinity of the CO $v_2 = 0 \to 1$ transition at 2143.2711 cm^{-1} (*3*). The density of states is high. $v_2 = 1$ states exist in a dense set of $v_2 = 0$ states. To label states, we compute the expectation value of $\hat{H}' = -\frac{1}{2\mu_{CO}}\frac{\partial^2}{\partial r_2^2} + V_{CO}(r_2)$. $v_2 = 1$ states have expectation values close to 1.5 ω_{CO}, where ω_{CO} is the CO fundamental frequency. The expectation values are obtained using the Hellmann-Feynman theorem by computing energy levels of the perturbed Hamiltonian $\hat{H}(\lambda) = \hat{H}_0 + \lambda\hat{H}'$, where $\hat{H}_0$ is the H_2-CO Hamiltonian and $\lambda = 10^{-5}$, following (*48*).

4D rovibrational bound and scattering calculations

We have used the BOUND and MOLSCAT programs (*32*) to perform the 4D rovibrational and scattering calculations. The rotational constants were the same as in (*2*, *20*): $B_0(H_2) = 59.322$ cm^{-1}, $B_0(CO) = 1.9225$ cm^{-1}, and $B_1(CO) = 1.9050$ cm^{-1} (*49*). The basis set and integration ranges were increased compared to (*2*, *20*): CO rotational quantum number j_2 from 8 to 12 (to 15 in scattering calculations), the partial wave expansion of the PES in BOUND/MOLSCAT was increased from $l = 10$ to 12, and the numerical integration step was decreased from 0.4 to 0.3 Å in the bound-state calculations and was equal to 0.05 bohr in the scattering calculations. The scattering energy was scanned with a step size of 10^{-4} cm^{-1}. Narrow resonances were first localized with the stabilization method and then scanned in scattering calculations with adaptive steps.

Supplementary Materials

This PDF file includes:

Fig. S1
Tables S1 to S7
Legends for codes S1 and S2

Other Supplementary Material for this manuscript includes the following:

Codes S1 and S2

REFERENCES AND NOTES

1. A. R. W. McKellar, High-resolution infrared spectrum and energy levels of the weakly bound complex, CO–*para*H_2. *J. Chem. Phys.* **108**, 1811–1820 (1998).
2. P. Jankowski, A. R. W. McKellar, K. Szalewicz, Theory untangles the high-resolution infrared spectrum of the *ortho*H_2–CO van der Waals complex. *Science* **336**, 1147–1150 (2012).
3. J. A. Coxon, P. G. Hajigeorgiou, Direct potential fit analysis of the $X^1\Sigma^+$ ground state of CO. *J. Chem. Phys.* **121**, 2992 (2004).
4. A. D. Bolatto, M. Wolfire, A. K. Leroy, The CO-to-H_2 conversion factor. *Annu. Rev. Astron. Astrophys.* **51**, 207–268 (2013).
5. E. B. Burgh, K. France, S. R. McCandliss, Direct measurement of the ratio of carbon monoxide to molecular hydrogen in the diffuse interstellar medium. *Astrophys. J.* **658**, 446–454 (2007).
6. S. C. O. Glover, M. Mac Low, On the relationship between molecular hydrogen and carbon monoxide abundances in molecular clouds. *Mon. Notice Royal Astron. Soc.* **412**, 337–350 (2011).
7. P. C. Clark, S. C. O. Glover, Does the CO-to-H_2 conversion factor depend on the star formation rate? *Mon. Notice Royal Astron. Soc.* **452**, 2057–2070 (2015).
8. R. J. Allen, L. Loinard, A. R. W. McKellar, J. Lequeux, A search for the CO–H_2 Dimer in the galaxy. *Astrophys. J.* **489**, 102–108 (1997).
9. A. Potapov, Á. Sánchez-Monge, P. Schilke, U. U. Graf, T. Möller, S. Schlemmer, The CO–H_2 van der Waals complex and complex organic molecules in cold molecular clouds: A TMC-1C survey. *Astro. Astrophys.* **594**, A117 (2016).
10. J. Kalirai, Scientific discovery with the James Webb Space Telescope. *Contemp. Phys.* **59**, 251–290 (2018).
11. M. Wernli, P. Valiron, A. Faure, L. Wiesenfeld, P. Jankowski, K. Szalewicz, Improved low-temperature rate constants for rotational excitation of CO by H_2. *Astro. Astrophys.* **446**, 367–372 (2006).
12. P. L. Raston, W. Jäger, H. Li, R. J. Le Roy, P. Roy, Persistent molecular superfluid response in doped para-hydrogen clusters. *Phys. Rev. Lett.* **108**, 253402 (2012).

13. P. Jankowski, K. Szalewicz, *Ab initio* potential energy surface and infrared spectra of H_2–CO and D_2–CO van der Waals complexes. *J. Chem. Phys.* **108**, 3554–3565 (1998).
14. A. Kudian, H. L. Welsh, A. Watanabe, Spectra of H_2–Ar, H_2–N_2, and H_2–CO van der Waals complexes. *J. Chem. Phys.* **47**, 1553–1554 (1967).
15. A. R. W. McKellar, Infrared spectra of the H_2–N_2 and H_2–CO van der Waals complexes. *J. Chem. Phys.* **93**, 18–24 (1990).
16. A. R. W. McKellar, Infrared spectra of CO–H_2 and CO–D_2 van der Waals complexes in the 4.7 μm region. *Chem. Phys. Lett.* **186**, 58–64 (1991).
17. R. Schinke, H. Meyer, U. Buck, G. H. F. Diercksen, A new rigid-rotor H_2–CO potential energy surface from accurate *ab initio* calculations and rotationally inelastic scattering data. *J. Chem. Phys.* **80**, 5518–5530 (1984).
18. Z. Bačič, R. Schinke, G. H. F. Diercksen, Vibrational relaxation of CO (n=1) in collisions with H_2. I. Potential energy surface and test of dynamical approximations. *J. Chem. Phys.* **82**, 236–244 (1985).
19. P. Jankowski, K. Szalewicz, A new *ab initio* interaction energy surface and high-resolution spectra of the H_2–CO van der Waals complex. *J. Chem. Phys.* **123**, 104301 (2005).
20. P. Jankowski, L. A. Surin, A. Potapov, S. Schlemmer, A. R. W. McKellar, K. Szalewicz, A comprehensive experimental and theoretical study of H_2–CO spectra. *J. Chem. Phys.* **138**, 084307 (2013).
21. I. Pak, L. A. Surin, B. S. Dumesh, D. A. Roth, F. Lewen, G. Winnewisser, Discovery of the rotational spectrum of the weakly bound complex CO–H_2. *Chem. Phys. Lett.* **304**, 145–149 (1999).
22. A. V. Potapov, L. A. Surin, V. A. Panfilov, B. S. Dumesh, T. F. Giesen, S. Schlemmer, P. L. Raston, W. Jäger, Rotational spectroscopy of the CO-*para*-H_2 molecular complex. *Astrophys. J.* **703**, 2108–2112 (2009).
23. P. Jankowski, Approximate generation of full-dimensional *ab initio* van der Waals surfaces for high-resolution spectroscopy. *J. Chem. Phys.* **121**, 1655–1662 (2004).
24. B. Yang, P. Zhang, X. Wang, P. C. Stancil, J. M. Bowman, N. Balakrishnan, R. C. Forrey, Quantum dynamics of CO–H_2 in full dimensionality. *Nat. Commun.* **6**, 6629 (2015).
25. A. Faure, P. Jankowski, T. Stoecklin, K. Szalewicz, On the importance of fulldimensionality in low-energy molecular scattering calculations. *Sci. Rep.* **6**, 28449 (2016).
26. G. Garberoglio, P. Jankowski, K. Szalewicz, A. H. Harvey, All-dimensional H_2–CO potential: Validation with fully quantum second virial coefficients. *J. Chem. Phys.* **146**, 054304 (2017).
27. P. Jankowski, E. Grabowska, K. Szalewicz, On the role of coupled-clusters' full triple and perturbative quadruple excitations on rovibrational spectra of van der Waals complexes. *Mol. Phys.* **119**, e1955989 (2021).
28. M. Jeziorska, P. Jankowski, K. Szalewicz, B. Jeziorski, On the optimal choice of monomer geometry in calculations of intermolecular interaction energies: Rovibrational spectrum of Ar–HF from two- and three-dimensional potentials. *J. Chem. Phys.* **113**, 2957–2968 (2000).
29. X.-G. Wang, T. Carrington Jr., Using monomer vibrational wavefunctions to compute numerically exact (12D) rovibrational levels of water dimer. *J. Chem. Phys.* **148**, 074108 (2018).
30. X.-G. Wang, T. Carrington Jr., New ideas for using contracted basis functions with a Lanczos eigensolver for computing vibrational spectra of molecules with four or more atoms. *J. Chem. Phys.* **117**, 6923–6934 (2002).
31. X.-G. Wang, T. Carrington Jr., J. Tang, A. R. W. McKellar, Theoretical and experimental studies of the infrared rovibrational spectrum of He_2–N_2O. *J. Chem. Phys.* **123**, 034301 (2005).
32. J. M. Hutson, C. R. Le Sueur, MOLSCAT, BOUND, and FIELD, version 2020.0 (2020); https://github.com/molscat/molscat.
33. F. Merkt, M. Quack, Handbook of high-resolution spectroscopy, in *Molecular Quantum Mechanics and Molecular Spectra, Molecular Symmetry, and Interaction of Matter with Radiation* (Wiley & Sons, 2011), vol. 1, pp. 1–55.
34. M. Zaborowski, M. Słowiński, K. Stankiewicz, F. Thibault, A. Cygan, H. Jóźwiak, G. Kowzan, P. Masłowski, A. Nishiyama, N. Stolarczyk, S. Wójtewicz, R. Ciuryło, D. Lisak, P. Wcisło, Ultrahigh finesse cavity-enhanced spectroscopy for accurate tests of quantum electrodynamics for molecules. *Opt. Lett.* **45**, 1603–1606 (2020).
35. M. Słowiński, M. Makowski, K. L. Sołtys, K. Stankiewicz, S. Wójtewicz, D. Lisak, M. Piwiński, P. Wcisło, Cryogenic mirror position actuator for spectroscopic applications. *Rev. Sci. Instrum.* **93**, 115003 (2022).
36. V. Babin, C. Leforestier, F. Paesani, Development of a "First Principles" water potential with flexible monomers: Dimer potential energy surface, VRT spectrum, and second virial coefficient. *J. Chem. Theory Comput.* **9**, 5395–5403 (2013).
37. B. Fernández, H. Koch, J. Makarewicz, Accurate intermolecular ground state potential of the Ar–N_2 complex. *J. Chem. Phys.* **110**, 8525–8532 (1999).
38. B. J. Braams, J. M. Bowman, Permutationally invariant potential energy surfaces in high dimensionality. *Int. Rev. Phys. Chem.* **28**, 577–606 (2009).
39. K. Pachucki, Born-Oppenheimer potential for H_2. *Phys. Rev. A* **82**, 032509 (2010).
40. L. Song, A. van der Avoird, G. C. Groenenboom, Three-dimensional ab initio potential energy surface for H–CO($\tilde{X}^2A'$). *J. Phys. Chem. A* **117**, 7571–7579 (2013).
41. A. Le Floch, Revised molecular constants for the ground state of CO. *Mol. Phys.* **72**, 133–144 (1991).
42. R. Chen, H. Guo, A single Lanczos propagation method for calculating transition amplitudes. II. Modified QL and symmetry adaptation. *J. Chem. Phys.* **114**, 1467–1472 (2001).
43. X.-G. Wang, T. Carrington Jr., A symmetry-adapted Lanczos method for calculating energy levels with different symmetries from a single set of iterations. *J. Chem. Phys.* **114**, 1473–1477 (2001).
44. R. Dawes, X.-G. Wang, A. W. Jasper, T. Carrington Jr., Nitrous oxide dimer: A new potential energy surface and rovibrational spectrum of the nonpolar isomer. *J. Chem. Phys.* **133**, 134304 (2010).
45. X.-G. Wang, T. Carrington Jr., R. Dawes, A. W. Jasper, The vibration–rotation–tunneling spectrum of the polar and T-shaped-N-in isomers of $(NNO)_2$. *J. Mol. Spectrosc.* **268**, 53–65 (2011).
46. H. Wei, T. Carrington Jr., The discrete variable representation of a triatomic hamiltonian in bond length–bond angle coordinates. *J. Chem. Phys.* **97**, 3029–3037 (1992).
47. J. Echave, D. C. Clary, Potential optimized discrete variable representation. *Chem. Phys. Lett.* **190**, 225–230 (1992).
48. R. Chen, H. Guo, A low-storage filter-diagonalization method to calculate expectation values of operators non-commutative with the Hamiltonian: Vibrational assignment of HOCl. *Chem. Phys. Lett.* **308**, 123–130 (1999).
49. K. P. Huber, G. Herzberg, *Molecular Spectra and Molecular Structure. IV. Constants of diatomic molecules* (Van Nostrand Reinhold, 1979).

Acknowledgments: We are grateful to A. R. W. McKellar for sharing with us raw data from the *ortho*H_2–CO experiment. **Funding:** This research was supported by the National Science Centre, Poland, grant no. 2017/25/B/ST4/01300 (to E.G., M.S., and P.J.), by the Natural Sciences and Engineering Research Council and The Digital Research Alliance of Canada (to X.-G.W. and T.C.), and by the National Science Foundation under grant nos. CHE-2154908 and CHE-2313826 (K.Sz.). **Author contributions:** Conceptualization: X.-G.W., T.C., K.S., and P.J. Calculations: M.S., E.G., X.-G.W., and P.J. Writing: M.S., X.-G.W., T.C., K.S., and P.J. **Competing interests:** The authors declare that they have no competing interests. **Data and materials availability:** All data needed to evaluate the conclusions in the paper are present in the paper and/or the Supplementary Materials.

Submitted 20 July 2023
Accepted 22 January 2024
Published 23 February 2024
10.1126/sciadv.adj8632